Heliyon 6 (2020) e04641

Contents lists available at ScienceDirect

Heliyon

journal homepage: www.cell.com/heliyon

Research article

Vibrational spectra, Hirshfeld surface analysis, molecular docking studies of (RS)-N,N-bis(2-chloroethyl)-1,3,2-oxazaphosphinan-2-amine 2-oxide by DFT approach

M. Govindammal, M. Prasath *

Department of Physics, Periyar University PG Extension Centre, Dharmapuri, 636701, India

ARTICLE INFO

Keywords:
Molecular physics
Quantum mechanics
Theoretical chemistry
DFT
FTIR
ADMET
Hirshfeld surface
Docking studies

ABSTRACT

The Cyclophosphamide (CYC) is used as an anti cancer agent. It is chemically known as (RS)-N,N-bis(2-chloroethyl)-1,3,2-oxazaphosphinan-2-amine 2-oxide. The vibrational assignments survey of the CYC was implemented by employing FT-IR and FT-Raman spectroscopic investigation and the results are compared with theoretical features. The optimized geometrical parameters, IR intensity and Raman Activity of the vibrational bands of CYC were determined from the B3LYP functional with 6–311++G (d, p) level of theory. In the current work, quantum chemical calculations were adopted to contemplate the vibrational assignments of CYC and the outcomes are compared with experimental findings. Molecular Electrostatic Potential (MEP) and HOMO-LUMO energies are very effective in the examination of charge transfer and distribution of the molecular structure. The molecular orbital contributions were evaluated by using the Total Density of States (TDOS). The analysis of Natural Bond Orbital (NBO), Mulliken population and Fukui function studies were done. Intermolecular interaction of the title compound was examined through Hirshfeld surface analysis. The evaluation of drug-likeness was accomplished in accordance with Lipinski's Rule of Five and molecular descriptors were utilized to predict the ADMET profiles of the CYC molecule. The recent research studies reports that the structural and bio-activity of the CYC was affirmed by the docking analysis of CYC with protein PI3K/AKT inhibitor, it acts as anti-lung cancer agent.

1. Introduction

Lung cancer is a prevalent malignancy and significant in causing cancer death in both male and female worldwide [1]. Cancer is generally caused by abnormal growth of cells, which potentially spread into other organs and tissues. The title compound is a drug known under trade name Cyclophosphamide (CYC) (also known as cytophosphane and cytoxan). It is approved for the treatment of different cancers such as lymphoma, multiple myeloma, leukemia, and small cell lung cancer etc., [2, 3]. CYC is preferred as the Non-Small Cell Lung Cancer (NSCLC) specialist [4]. CYC metabolites are mainly excreted in the pee unaltered, and drug dosing should be suitably adjusted in the setting of renal brokenness [5]. The molecular formula is $C_7H_{15}Cl_2N_2O_2P$ with molecular mass 261.086 g/mol.

Generally PI3K/AKT inhibitors pathway plays a significant part in biological activity. This signaling network has been related with several cellular processes critical to the initiation and during the survival, metabolism and cancer growth [6, 7]. It plays a considerable role in apoptosis, survival and angiogenesis [8, 9]. As a result, this signaling network could be a major target in cancer inhibition. An imbalance in the PI3K/AKT pathway make an important contribution in the arrangement and growth of lung cancer, and the activation of the PI3K/AKT pathway can stimulate the transduction of many downstream signals and assist the growth of NSCLC [10, 11, 12]. Targeting such intracellular pathways that modulate proliferation, apoptosis, metastasis and resistance to chemotherapy shows a significant therapeutic approach for lung cancer. Therefore inhibiting the PI3K/AKT signaling pathways has been represented to be the principal targets in lung cancer treatment. AKT, alongside phosphatidyl inositol 3-kinase (PI3K), are the crucial components of the Tyrosine Kinase signaling network and it is called as PI3K/AKT signaling, this signaling transduction way triggers the cell survival and growth factors development to extracellular signals [13].

In the current exploration, CYC compound was optimized at the DFT/B3LYP [14] functional using the extended 6–311++G (d,p) level of theory. The vibrational frequencies of the molecule were also computed at B3LYP functional and vibrational assignments were prepared with the

* Corresponding author.
E-mail address: sanprasath2006@gmail.com (M. Prasath).

https://doi.org/10.1016/j.heliyon.2020.e04641
Received 25 April 2020; Received in revised form 11 June 2020; Accepted 3 August 2020
2405-8440/© 2020 The Author(s). Published by Elsevier Ltd. This is an open access article under the CC BY-NC-ND license (http://creativecommons.org/licenses/by-nc-nd/4.0/).

assistance of computed (using PED- Potential Energy Distribution program) and experimental values. The both HOMO-LUMO energies demonstrate the biochemical activity of CYC. The stability and donor-acceptor interaction of the CYC was inspected by natural bonding orbital (NBO) study. The charge distribution and chemical reactivity region of the CYC compound have been represented by Molecular Electrostatic Potential (MEP) map. Fukui function and Mulliken population were done to identify the electronegative and electropositive atoms in the compound. The intermolecular interaction and two dimensional (2D) finger print plots of CYC molecules are executed by Hirshfeld surface survey. ADMET (Absorption, Distribution, Metabolism, Excretion and Toxicity) properties were utilized to calculate the pharmacokinetic characteristics of the CYC molecule. In addition drug-likeness properties were studied and the compound obeys Lipinski's rule of five. Docking of ligand (CYC) in the receptor binding site of target protein (PI3K/AKT inhibitor) and calculation of flexible binding affinity of the stable complex is the primary role in structure based and assigned drug model. The amino acid residues in the binding cavity of PI3K/AKT protein, contributes more interaction other than hydrogen bonding interactions of CYC molecule and the lowest binding energy of CYC have been examined with the assistance of docking studies.

2. Experimental details

The compound was bought from Sigma Aldrich Company with 98% purity and utilized as such without additional refinement. FT-IR spectrum of CYC was precisely recorded through PERKIN ELMER (resolution range 1.0cm^{-1} and scale region 4000-450cm^{-1}) evacuation mode with a KBr method. Further FT-Raman spectrum has been recorded in the 4000-100 cm^{-1} scale region by BRUCKER RFS 27 with the resolution of 2 cm^{-1} using Nd-YAG laser at SAIF, IIT, and Chennai, India.

3. Computational details

The quantum chemical calculation were done with the B3LYP functional, 6–311++G (d,p) level of theory employing Gaussian 09W Program package [15]. Further the structurally optimized compound was viewed by using Gaussview 5.0 software [16]. The molecular structure is optimized and employed for the calculation of vibrational assignments, Raman activities and IR intensities and computation of the Potential Energy Distribution (PED) were calculated utilizing the VEDA 4.0 program [17]. Accordingly, we have utilized a scaling factor estimation of 0.961 for the B3LYP/6–311++G (d,p) level of theory [18, 19]. The geometric structural parameters like bond length and bond angle were calculated. Gaussview was utilized to determine the Molecular electrostatic potential map (MEP) [20]. The donor-acceptor interactions in the natural bond orbitals (NBO) were calculated to second- order Fock matrix [21]. The paper further explains charge distribution analysis and electronic property with HOMO-LUMO energy gap. Hirshfeld surface estimations were performed using Crystal explorer 17.5 program packages [22]. Molecular docking analysis was executed with AUTODOCK 1.5.6 software [23]. PyMOL [24] chimera [25] program were utilized to visualize the protein-ligand complex and intermolecular interaction of PI3K/AKT inhibitor and CYC ligand molecule.

4. Result and discussion

4.1. Molecular geometry

Optimized geometrical parameters of the CYC molecule are reported in Table 1 and optimized molecular structure with labeling of atoms is presented in Figure 1. The theoretical values for the CYC molecule were observed as strongly identified and compared with experimental data as presented in Table 1 [26]. As of the single crystal XRD data, it is found that CYC molecule belongs to the orthorhombic crystal system with the following cell dimensions; a = 9.9062 Å; b = 9.8380 Å; c = 24.061 Å. The distinction between the experimental and theoretical values can mainly be ascribed to the way that calculations were executed utilizing segregated molecule in the gaseous state to accomplish theoretical values and in solid state for experimental values. The bond lengths C (21)–Cl (27) and C (24)-Cl (28) are found to be 1.815 Å (Theoretical) and slightly deviated from the experimental value (1.791 Å). The calculated bond length P (13)–N (14) is found to be 1.669 Å which is in good accord with the experimental value 1.641 Å as seen from Table 1. The calculated and experimental bond angle values of N (10)-P (13)-N (14) of CYC is 107.05 Å and 105.76 Å respectively. This divergence in bond lengths and bond angle implies the bonding nature of atom.

4.2. Vibrational spectral analysis

The CYC molecules possess C_1 symmetry group and possess 29 atoms with 81 normal modes of vibrations detailed. The spectral investigation of the noticed FT-IR and FT-Raman spectra and theoretically speculated spectra of both are made known in Figure 2 (a&b) respectively. The observed and determined frequencies are introduced in Table S1. The PED for every ordinary mode among the symmetry coordinates of the molecule was determined. As a final point, complete assignments of the fundamental were proposed dependent on the determined PED values.

4.2.1. CH vibrations

The aromatic stretching CH vibration wave numbers show up in the region 3100-3000 cm^{-1} which are the property range for the rapid recognizable proof of CH stretching vibrations [27, 28]. These bands of the title compound appear in the region 3046, 3035, 2996, 2994, 2991, 2983, 2975, 2974, 2956, 2944, 2926, 2916, 2913 and 2911cm^{-1}. The CH stretching vibration modes are noticed at 3086, 2961 and 2881 cm^{-1} experimentally observed in the FT-IR spectrum and at 3030, 2965, 2895 and 2893 cm^{-1} in the FT-Raman spectrum. The CH vibrations are supported by a maximum Potential Energy Distribution contribution of 95%.

4.2.2. NH vibrations

The NH stretching vibrations are commonly found in the range 3500–3300 cm^{-1} [29]. CYC has its stretching modes which always appear in higher wave numbers and it is referenced theoretically and experimentally in Table S1 with Potential Energy Distribution (PED) as 99%. Experimental peak value detected at 3486 cm^{-1} (FTIR) and 3481 cm^{-1} (FT-Raman) are confined to NH vibrations. The theoretical scaled frequency of NH vibration mode appears at 3450 cm^{-1} which agrees well with experimental value.

4.2.3. CC vibrations

The ring (CC) vibration is mostly found in the range of 1600–1400 cm^{-1} [13,30,31]. In the current examination, the CC bands which are of various intensities were monitored at 1430 cm^{-1} in FT-IR range. FT-Raman bands were diagnosed at 1444, 1438, and 1424 cm^{-1}. The theoretical data were acquired at 1446, 1440, 1437 and 1424 cm^{-1} by B3LYP functional 6–311++G (d,p) level of theory. It illustrates that the theoretical data are in meaningful compromise with experimental data. The maximum PED contribution is 81%.

4.2.4. CN vibrations

Recognizable proof of CN vibration is a problematic errand as the blending of band is conceivable in the indicated region. Three CN vibrations were reported for the title compound. CN vibrations are probable to appear in the range of 1386–1266 cm^{-1} [32]. In the present work, computed CN stretching vibrations are accounted in 1452, 1433 and 1418 cm^{-1}. FT-IR bands were detected at 1454 cm^{-1} and 1468 cm^{-1} in the FT-Raman range appears as a broadband. It is upheld with a normal PED contribution of 62%.

Table 1. Optimized geometrical parameters (bond length (Å) and bond angle (°)) for CYC.

parameters	calculated	Experi[a]	parameters	Calculated	Experi[a]
Bond length Å			Bond angle (°)		
C (2)–H (4)	1.095	0.989	C (2)-C (1)-H (5)	110.13	109.04
C (2)–H (9)	1.095	0.990	C (2)-C (1)-C (6)	111.11	111.19
C (2)–C (3)	1.528	1.525	C (2)-C (1)-N (10)	112.84	112.56
C (24)–H (26)	1.088	0.990	H (5)-C (1)-C (6)	106.94	109.58
C (24)–H (25)	1.089	0.989	H (5)-C (1)-N (10)	107.41	109.09
C (21)–H (23)	1.087	0.990	C (6)-C (1)-N (10)	108.16	108.56
C (21)–H (22)	1.088	0.990	C (1)-C (2)-C (3)	111.72	111.19
C (18)–C (21)	1.526	1.514	C (1)-C (2)-H (4)	109.84	109.04
C (18)–H (20)	1.090	0.989	C (1)-C (2)-H (9)	109.79	109.14
C (18)–H (19)	1.092	0.991	C (3)-C (2)-H (4)	108.60	109.42
C (15)–H (17)	1.090	0.990	C (3)-C (2)-H (4)	109.42	109.43
C (15)–H (16)	1.095	0.991	C (3)-C (2)-H (9)	107.36	109.58
C (24)–C (15)	1.528	1.518	C (2)-C (3)-H (7)	111.10	109.42
C (3)–H (7)	1.095	0.990	C (2)-C (3)-H (8)	111.58	109.43
C (3)–H (8)	1.089	0.989	C (2)-C (3)-O (12)	111.55	109.63
C (1)–C (2)	1.536	1.514	H (7)-C (3)-H (8)	108.45	108.21
C (1)–H (5)	1.093	0.991	H (7)-C (3)-H (8)	108.56	110.10
C (1)–H (6)	1.091	0.989	H (8)-C (3)-O (12)	105.37	109.60
C (3)–O (12)	1.452	1.462	C (1)-N (10)-H (11)	112.79	117.54
N (10)–C (1)	1.480	1.478	C (1)-N (10)-P (13)	114.58	119.99
N (10)–H (11)	1.013	0.789	H (11)-N (10)-P (13)	114.00	115.56
N (14)–C (15)	1.466	1.463	C (3)-O (12)-P (13)	117.17	117.50
N (14)–C (18)	1.476	1.462	N (10)-P (13)-O (12)	103.12	101.85
C (24)–Cl (28)	1.815	1.791	N (10)-P (13)-N (14)	107.05	105.82
C (21)–Cl (27)	1.816	1.789	N (10)-P (13)-O (29)	113.76	110.85
P (13)–O (12)	1.635	1.588	O (12)-P (13)-N (14)	103.40	101.85
P (13)–O (29)	1.481	1.475	O (12)-P (13)-O (29)	114.59	112.30
P (13)–N (10)	1.691	1.633	N (14)-P (13)-O (29)	113.81	119.29
P (13)–N (14)	1.669	1.641	P (13)-N (14)-C (15)	122.19	120.37
			P (13)-N (14)-C (18)	117.94	120.05
			C (15)-N (14)-C (18)	117.77	118.13
			N (14)-C (15)-H (16)	109.96	109.68
			N (14)-C (15)-H (17)	109.10	109.75
			N (14)-C (15)-C (24)	111.85	109.77
			H (16)-C (15)-H (17)	106.55	108.02
			H (16)-C (15)-C (24)	109.62	109.34
			H (17)-C (15)-C (24)	109.62	109.39
			N (14)-C (18)-H (19)	107.93	108.56
			N (14)-C (18)-H (20)	110.20	108.57
			N (14)-C (18)-C (21)	111.66	114.85
			H (19)-C (18)-H (20)	107.84	108.21
			H (19)-C (18)-C (21)	110.11	109.68
			H (20)-C (18)-C (21)	109.02	109.73
			C (18)-C (21)-H (22)	112.23	109.43
			C (18)-C (21)-H (23)	110.95	110.01
			C (18)-C (21)-Cl (27)	110.06	108.30
			H (22)-C (21)-H (23)	110.00	110.06
			H (22)-C (21)-Cl (27)	106.56	108.41
			H (23)-C (21)-Cl (27)	106.81	109.95
			C (15)-C (24)-H (25)	111.78	109.36
			C (15)-C (24)-H (26)	112.19	109.36
			C (15)-C (24)-Cl (28)	110.20	111.26
			H (25)-C (24)-H (26)	109.29	108.00
			H (25)-C (24)-Cl (28)	106.85	109.36

[a] Experimental Values taken from ref. [26].

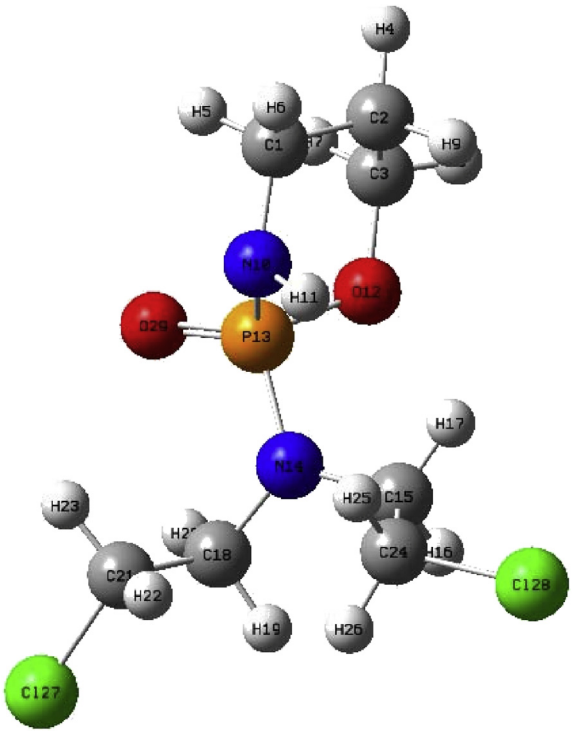

Figure 1. Optimized geometric structure with atom numbering of CYC.

Table 2. Calculated energy values of CYC by B3LYP/6–311++G (d,p) method.

Parameters	values
HOMO energy (E_{HOMO})	-6.4687
LUMO energy (E_{LUMO})	-0.2377
Energy gap (eV)	6.2309
Ionization potential (I)	6.4687
Electron affinity (A)	0.2377
Electronegativity (χ)	3.3532
Chemical potential (μ)	-3.3532
Chemical Hardness (η)	3.1155
Chemical softness (S)	0.1604
Electrophilicity (ω)	1.8045

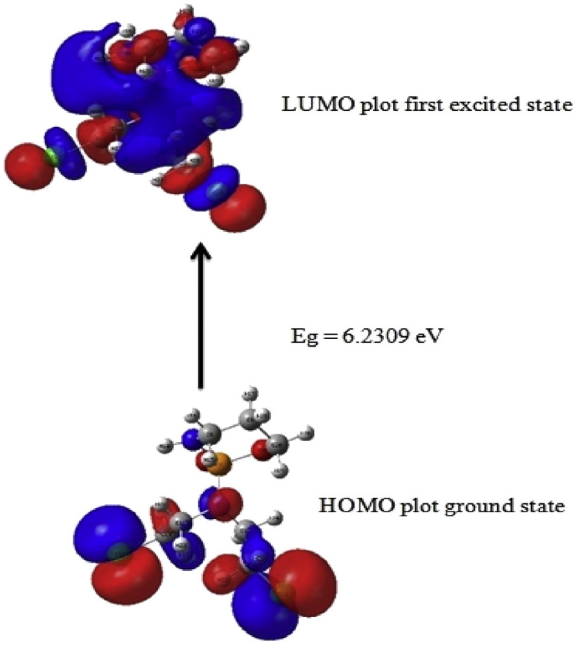

Figure 3. Atomic orbital HOMO-LUMO composition of the frontier molecular orbital of CYC.

4.2.5. Other vibrations

In bending vibrations of HCH, the theoretical estimations of the CYC molecule were seen in the region 1245, 1243, 1211, 1172, 1083,1048 and 1007 cm $^{-1}$. The HCH bending peak appears at 1044 cm^{-1} in FTIR and in FT-Raman band it appears at 1042 cm^{-1}. The most extreme Potential Energy Distribution of 89%.

In HCC vibration of band occurs in the region 1227, 1085, 1057 and 1020 cm^{-1}. The experimental HCC vibration located at 1112 cm $^{-1}$ in FTIR and Raman bands are recorded at 1222 cm $^{-1}$, respectively. The PED contribution is 63%.

The other bending vibrations (HNP, HCN, CCC, HCO, CNP and NPO) were observed for the CYC molecule and furthermore the torsion vibrations of CCCl, HCCN, HCCC, CCOH, CCCC, HCNP, and HCCH were also noticed in the CYC molecule. All the vibrations of CYC were processed and the observed values are in positive concurrence with the experimental values [33, 34, 35].

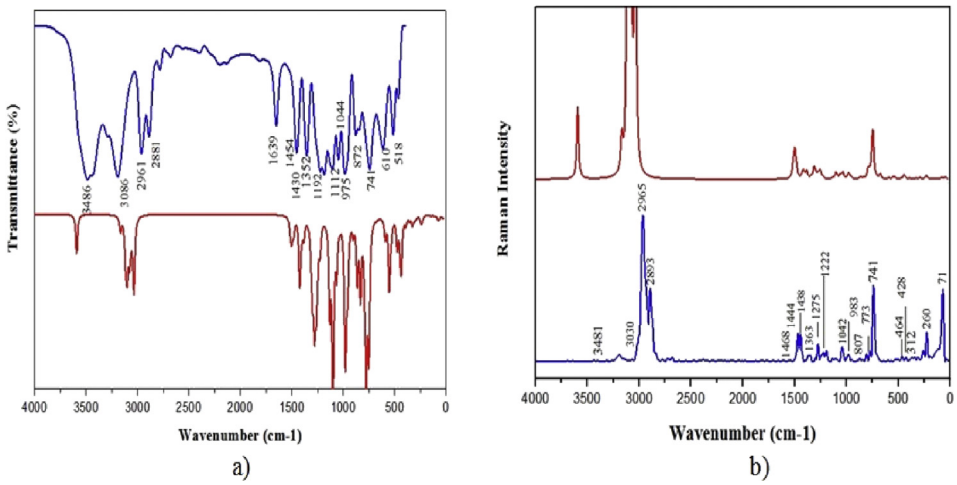

Figure 2. Experimental and calculated a) FT- IR and b) FT-Raman spectra of CYC.

Table 3. Mulliken Charge distribution and Fukui Function of CYC.

Atoms	Mulliken Atomic Charges			Fukui Function			
	N	N+1	N-1	f+	f	f^0	Δf(r)
C1	-0.369	-0.396	0.264	0.027	-0.633	0.660	0.660
C2	-0.151	-0.185	0.532	0.034	-0.683	0.717	0.717
C3	-0.281	-0.303	0.068	0.022	-0.349	0.371	0.371
H4	0.172	0.226	-0.580	-0.054	0.751	-0.805	-0.805
H5	0.226	0.269	0.108	-0.044	0.118	-0.162	-0.162
H6	0.184	0.237	-0.763	-0.053	0.947	-1.000	-1.000
H7	0.199	0.242	0.131	-0.043	0.068	-0.111	-0.111
H8	0.193	0.241	-0.268	-0.048	0.461	-0.509	-0.509
H9	0.144	0.183	-0.214	-0.039	0.357	-0.397	-0.397
N10	-0.386	-0.280	-0.376	-0.106	-0.010	-0.096	-0.096
H11	0.320	0.364	0.006	-0.044	0.315	-0.359	-0.359
O12	-0.178	-0.107	-0.224	-0.071	0.046	-0.117	-0.117
P13	0.262	0.176	1.065	0.086	-0.803	0.889	0.889
N14	-0.090	0.009	-0.028	-0.099	-0.062	-0.037	-0.037
C15	-0.480	-0.516	-0.760	0.037	0.280	-0.244	-0.244
H16	0.201	0.251	-0.007	-0.050	0.208	-0.258	-0.258
H17	0.127	0.161	0.197	-0.034	-0.070	0.036	0.036
C18	-0.507	-0.542	-0.339	0.035	-0.169	0.203	0.203
H19	0.117	0.172	0.044	-0.055	0.073	-0.128	-0.128
H20	0.219	0.259	0.239	-0.040	-0.020	-0.020	-0.020
C21	-0.449	-0.478	-0.122	0.029	-0.326	0.355	0.355
H22	0.187	0.213	0.004	-0.025	0.184	-0.209	-0.209
H23	0.242	0.257	0.168	-0.015	0.074	-0.089	-0.089
C24	-0.457	-0.463	0.574	0.006	-1.031	1.037	1.037
H25	0.157	0.169	-0.597	-0.012	0.754	-0.766	-0.766
H26	0.187	0.217	0.020	-0.030	0.167	-0.197	-0.197
Cl27	0.203	0.349	0.089	-0.146	0.114	-0.260	-0.260
Cl28	0.165	0.277	-0.022	-0.112	0.187	-0.299	-0.299
O29	-0.158	-0.003	-0.208	-0.155	0.050	-0.205	-0.205

4.3. Electronic properties

HOMO-LUMO energy gap of the CYC molecule is computed by using B3LYP functional with employing 6–311++G (d,p) level of theory which helps us to represent the chemical properties and kinetic stability of the molecule [36]. The Highest Occupied Molecular Orbital (HOMO) is the orbital that principally acts an electron-donor (e/d) and the Lowest Unoccupied Molecular Orbital (LUMO) is the orbital that principally acts as an electron-acceptor (e/a) [37]. HOMO-LUMO parameters are specified in (Table 2) which can be obtained from the following equations:

$$\text{Chemical potential } (\mu) = \frac{1}{2}(E_{LUMO} + E_{HOMO})$$

$$\text{Chemical Hardness } (\eta) = \frac{1}{2}(E_{LUMO} - E_{HOMO})$$

$$\text{Chemical softness } (S) = \frac{1}{2}\eta$$

$$\text{Electronegativity}(\chi) = -\frac{1}{2}(E_{LUMO} + E_{HOMO}) = -\mu$$

$$\text{Electrophilicity}(\omega) = \frac{\mu^2}{2\eta}$$

The HOMO-LUMO energy esteems are associated to the Ionization potential (I) and Electron affinity (A) of the molecule. In addition other parameters such as Chemical Potential (μ), Chemical Hardness (η), Chemical Softness (S), Electronegativity (χ) and Electrophilicity (ω) were predicted for the CYC molecule, evaluated by the DFT methods as shown in Figure 3 and the results are presented in Table 2. The computed HOMO-LUMO energy gap value is 6.2309 eV, the chemical hardness is also good criterion to display chemical stability. The higher chemical hardness and lower softness value shows the stability of the molecule. The chemical hardness of the compound was noted to be 3.1155 and softness value is 0.1604. The lower electrophilicity index value is 1.8045, which indicates the biological activity of the title compound [38].

4.4. Density of state analysis

The Neighboring orbitals may signify quasi-degenerate energy levels in the limit locale. In such cases, thought of just the HOMO and LUMO may not produce a practical explanation of the frontier orbitals. Therefore, the aggregate (TDOS), partial (PDOS) and overlap population

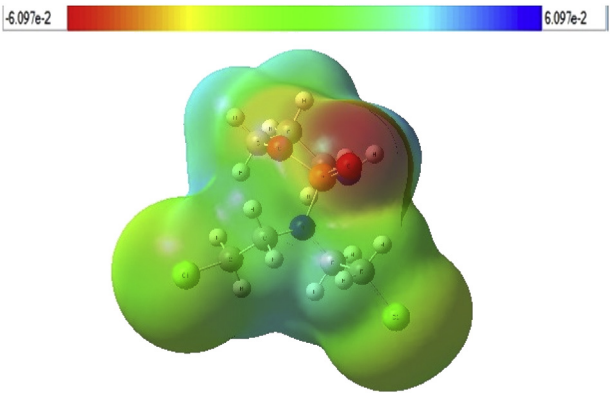

Figure 4. Molecular Electrostatic potential (MEP) of CYC.

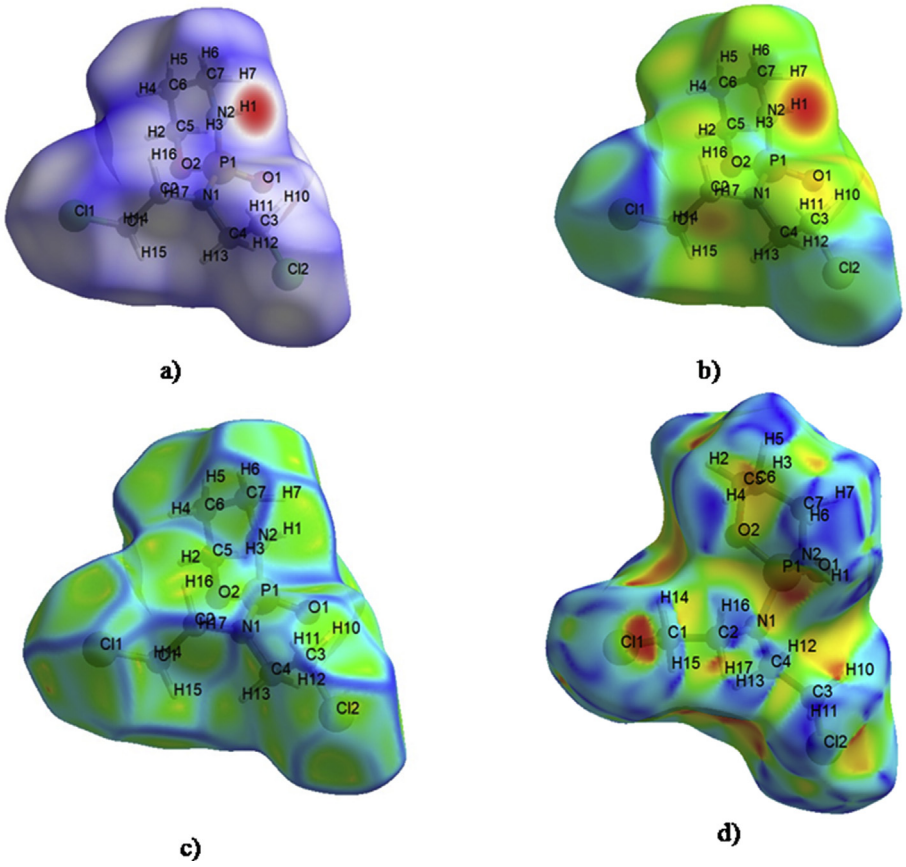

Figure 5. Hirshfeld surface mapped on (a) d_{norm}, (b) d_i, (c) curvedness, (d) shape index of CYC.

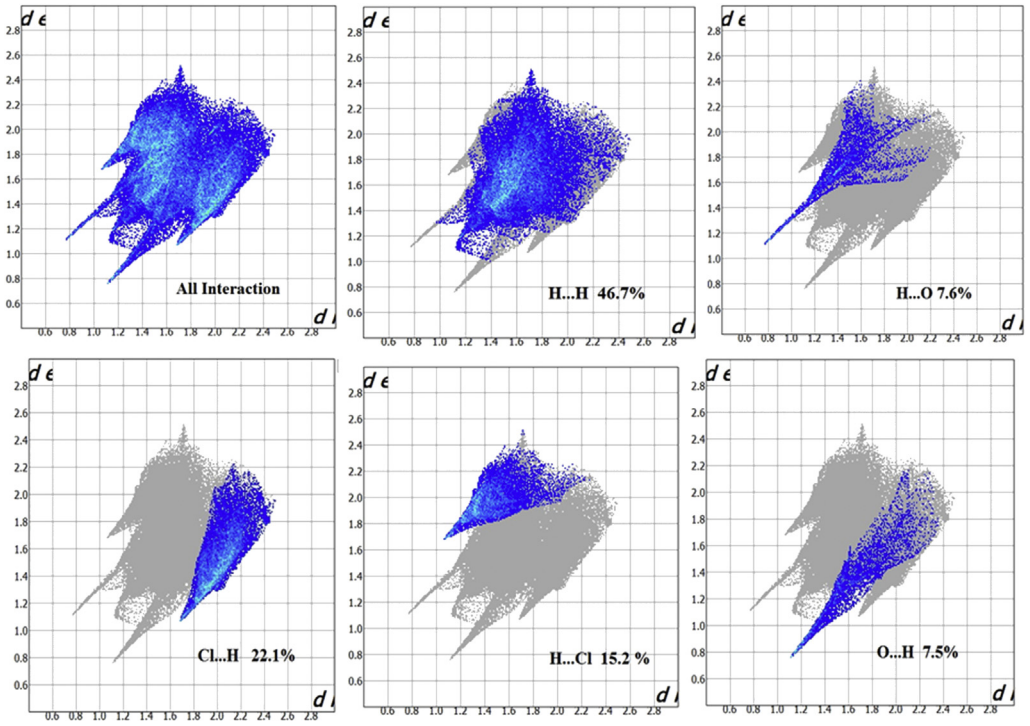

Figure 6. 2D Fingerprint plot resolved into H···H, H···O and H···Cl contacts showing the percentages of contacts and their relative contributions.

Table 4. Selected donor-acceptor interactions of CYC and their second order perturbation energies.

Donor(i)	Type	ED/e	Acceptor(j)	Type	ED/e	E (2)[a](kj mol-1)	E(J)[b]-E(i) (a.u)	F (i,j)[c](a.u)
σ	C1–C2	1.9881	σ*	C3–H8	0.01691	1.39	1.02	0.034
σ	C1–H5	1.9812	σ*	C2–H9	0.01618	2.7	0.9	0.044
σ	C1–H6	1.9827	σ*	N10–P13	0.15943	3.14	0.76	0.045
σ	C1–N10	1.9897	π*	P13–O29	0.15006	1.17	1.16	0.034
σ	C3–O12	1.9888	π*	P13–O29	0.15006	4.52	1.24	0.069
σ	N10–H13	1.9629	π*	P13–O29	0.15006	3.81	1.12	0.06
σ	O12–P13	1.9259	π*	P13–O29	0.15006	36.51	1.18	0.189
σ	P13–N14	1.886	σ*	N10–P13	0.15943	6.33	0.92	0.069
σ	P13–N14	1.886	σ*	O12–P13	0.16414	24.3	1.02	0.142
σ	P13–N14	1.886	π*	P13–O29	0.15006	70.11	1.09	0.249
σ	P13–O29	1.9755	σ*	O12–P13	0.16414	7.02	1.26	0.087
π	P13–O29	1.9293	σ*	N10–P13	0.15943	1.45	0.55	0.026
π	P13–O29	1.9293	σ*	O12–P13	0.16414	13.07	0.65	0.084
π	P13–O29	1.9293	σ*	P13–N14	0.08755	21.93	0.76	0.116
σ	N14–C15	1.9833	π*	P13–O29	0.15006	4.49	1.16	0.067
σ	C15–H17	1.9793	σ*	N14–C18	0.02534	3.94	0.85	0.052
σ	C15–H17	1.9793	σ*	C24–H26	0.02005	2.59	0.91	0.043
σ	N10	1.9995	σ*	O12–P13	0.16414	7.13	0.65	0.062
LP (2)	O12	1.9096	σ*	P13–O29	0.07438	9.11	0.7	0.071
LP (1)	N14	1.8364	σ*	N10–P13	0.15943	8.49	0.52	0.059
LP (2)	Cl28	1.9773	σ*	C24–H26	0.02005	3.52	0.7	0.044
LP (2)	O29	1.979	σ*	N10–P13	0.15943	19.47	0.5	0.089
LP (2)	O29	1.8127	σ*	O12–P13	0.16414	10.38	0.6	0.071

ED(e) is the electron density of donor and acceptor in the NBO analysis.
* Antibonding.
[a] *E* (2) means the energy of hyper conjugative interactions (stabilization energy).
[b] Energy difference between donor and acceptor *i* and *j* NBOs.
[c] *F* (*i*,*j*) is the Fock matrix element between *i* and *j* NBOs.

Table 5. Prediction of ADMET profiles for CYC.

A	B	C	D	E	F	G	H	I
0.3849	Non	94.322	25.672	-3.9795	Suitable	Qualified	Mutagen	Violated

A:ADMET_BBB.
B: P-glycoprotein inhibitor.
C: Human intestinal absorption (HIA+, %).
D: Plasma protein binding (PPB, %).
E: ADMET_SK logP.
F: Lipinski's rule.
G:CMC-like rule.
H:Ames_test.
I: Lead-like rule.

(OPDOS or COOP (Crystal Orbital Overlap Population)) density of states [39, 40, 41] were analyzed. The TDOS, PDOS and OPDOS are plotted in Figs.S1 (a, b &c) respectively. The most significant utilization of the DOS charts is to exhibit MO structures and their contribution to the chemical bonding through the OPDOS plots which are likewise mentioned in the writing as COOP diagram. The OPDOS shows the bonding, anti-bonding and nonbonding nature of the interaction of the two collaboration orbitals, atoms and groups. A positive estimation of the OPDOS shows a binding interaction, negative value implies that there is an anti-bonding interaction and zero value shows that the non-bonding interaction. As observed from Fig.S1, HOMO orbitals are limited on the ring and their contributions are about 95%. The LUMO orbitals are confined on the ring (75%) of the compound. N with H (Yellow line) is profoundly overlapped the orbital contrasted and other overlapped (O, Cl, C and P) orbitals. C with H (Green line) is humble overlapped the orbital as contrasted and other overlapped (N, Cl, O and P) orbitals.

Table 6. Drug likeness parameters of CYC.

Descriptors	Values
Hydrogen bond donor (HBD)	1
Hydrogen bond acceptor (HBA)	4
Partition coefficient (Mi logP)	0.76
Molecular weight (MW)	261.09
Topological polar surface area (TPSA) (Å2)	41.57
Number of atoms	29
Number of rotatable bonds	5

4.5. Mulliken analysis

Mulliken charge analysis manipulated the molecular properties such as polarizability and change in dipole moment of chemical bonds displayed in the molecule. The Mulliken atomic charge distribution of the CYC molecule estimated by B3LYP/6–311++G (d,p) level is listed in Table 3 and the graphical representation of the same is shown in Fig.S2.

Table 7. The biding affinity values of different possess of the CYC molecule with PI3/AKT inhibitor.

Mode	Binding affinity kcal/mol	Distance from best mode Å	
		RMSD l.b	RMSD u.b
1	-5.7	0.000	0.000
2	-5.7	0.674	2.669
3	-5.3	25.35	25.86
4	-5.1	20.61	21.576
5	-5.1	2.103	3.676
6	-5.0	20.788	21.709
7	-5.0	20.557	21.651
8	-4.9	25.366	25.987
9	-4.8	2.900	4.598

*RMSD l.b shows RMSD lower bond, while **RMSD u.b shows RMSD upper bond.

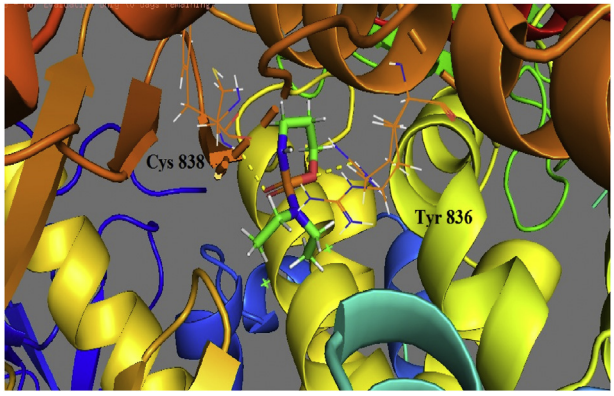

Figure 7. Docking and hydrogen bond interaction of CYC molecule with PI3K/AKT inhibitor.

Table 3 reveals the Mulliken atomic charge values of C, N, O, Cl, P and H atoms. The positive values have been acquired from the electropositive atoms such as H_{11}, H_{23} and P_{13}.The Fig.S2 represents the charge distribution of the CYC molecule which concludes that the hydrogen atoms are positively charged. From Fig S2, it can be seen that the maximum atomic charge values are retrieved for C_{18} (-0.507) atom. The atom P_{13} has been linked to the electronegative atoms like O_{12}, O_{29} N_{10} and N_{14}. So that, it holds negative value. Additionally, all oxygen, Chlorine and nitrogen atoms show negative charge.

4.6. Local reactivity descriptors analysis

The electron density dependent on the local reactivity descriptors are utilized to find the positive reactive locals of the molecule and it is significant in structuring the biological compound. The Fukui function encourages one to measure the most reactive site for electrophilic and nucleophilic attack within a molecule [42, 43, 44]. In the current work, local reactivity descriptors like Fukui (f^+, f^- &f^0) and Mulliken atomic charges were computed for the title molecule are presented in Table 3. Fukui work indicates the more reactive locales leads to the chemical effects in a molecule. From Table 3 its found to be C1, C2, C3, P13, H17, C18, C21 and C24 are the sites for nucleophilic attack and the other hand N10, N14, O12, O29, C15, Cl27 and Cl28 are the sits for electrophilic attack.

4.7. Electrostatic potential and Hirshfeld surface analysis

Electrostatic potentials mapped on Hirshfeld surfaces give direct insight into intermolecular interactions in crystals [45]. The molecular electrostatic potential (MEP) map exhibits electrostatic potential regions of the molecules by means of simple colour coding of the maps which lies from -6.097 $\times$ 10^{-2} a. u (deepest red) to 6.097 $\times$ 10^{-2} a. u (deepest blue). MEP is used to discover the electrophilic and nucleophilic attacks during the reactions as well as hydrogen bonding interactions. Besides, blue and red colours represent the positive and negative potentials, respectively Figure 4. The negative electrostatic potential is usually incorporated with the lone pair of electronegative atoms.

Hirshfeld surfaces gives, the molecular surface analysis d_{norm}, d_e, curvedness and shape index for CYC molecule as shown in Fig .5. The d_{norm} surface (Figure 5a) is a normalized contact distance, ranging from [-0.551 Å (red) to 1.515 Å (blue)]. The color code was employed (short d_{norm} range for red and long d_{norm} range for blue) respectively. The d_e surface of Figure 5b shows the distance between the nearest nuclei external to the surface region (0.7733–2.5377 Å). The shape index surface (Figure 5c) shows the electron density surface curves around the molecular interaction range from -1 Å to 1 Å [46, 47]. The curvedness Figure 5d indicates the electron density surface curves around the molecular interaction range (-4 Å to 4 Å) respectively. Hirshfeld surface analysis red color region have longer intermolecular interaction which represents the positive d_{norm} value, blue color region indicates shorter intermolecular contacts denoted as negative d_{norm} value and white color region with a d_{norm} value of zero. Hirshfeld surface analysis mapped on shape index and curvedness was carried out and is shown as conformation of the functional group in the molecule. The 2D Fingerprint plot resolved into H···H, H···O and H···Cl contacts showing the percentages of contacts and their relative contribution as shown in the Figure 6. The maximum and minimum contributions are H···H (46.7%) and O···H (7.5%) respectively. Other relative contributions of intermolecular interactions are Cl···H (22.1%), H···O (7.6%) and H···Cl (15.2%). The result affirms CYC molecule has supermolecular feature.

4.8. Donor- acceptor interactions

The NBO analysis is the mostly efficient method to explain intramolecular-intermolecular bonding, charge transfer, conjugative interactions and stabilization energy in the molecular system [48, 49]. This analysis has been done on the CYC molecule and listed in Table 4. The NBO analysis is performed to find the electron donor-electron acceptor interaction energy in the CYC molecule. The second order Fock matrix was finalized to calculate the donor-acceptor interaction in the NBO analysis. The stabilization energy E (2) for each electron-donor (i) and electron-acceptor (j) were done.

The intermolecular hyper conjugative interactions are (O12–P13) σ to (P13–O29) σ*, (P13–N14) σ to (P13–O29) π* and (P13–O29) π to (P13–N14) σ* shows the highest stabilization energies 36.51, 70.11 and 21.93 kJ/mol with ED/e 1.925 e, 1.886 e and 1.929 e. Another data is obtained from, LP(O12) to (P13–O29) π*, LP(O29) to σ*(N10–P13) and LP(N14) to (N10–P13) π* by stabilization energy value of 9.11, 19.47 and 8.49 kJ/mo with ED/e value 1.909 e, 1.979 e and 1.836 e, respectively.

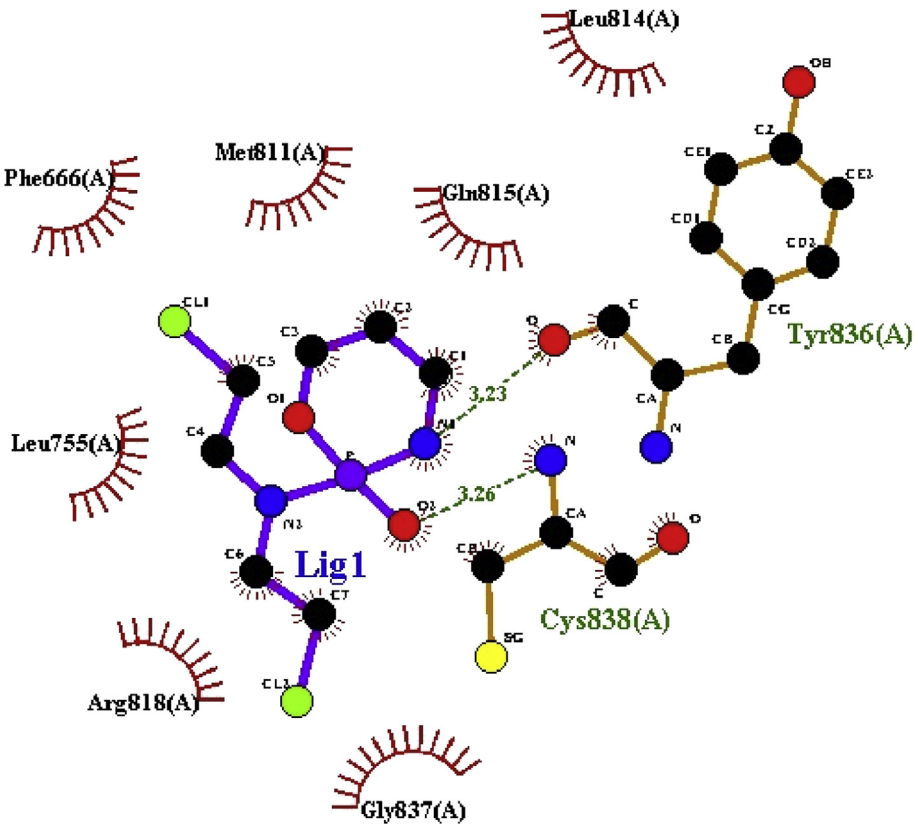

Figure 8. The ligplot showing intermolecular interaction of CYC molecule in the active site of PI3K/AKT inhibitor.

4.9. ADMET prediction

ADMET (Absorption, Distribution, Metabolism, Excretion and Toxicity) properties are helpful examinations in medicinal science for the piece of a molecule as drug-like were performed for the CYC molecule [50]. Every potential drug molecule needs to be tested for ADMET properties and properties are follows: the penetration through the Blood Brain Barrier (BBB) [51], P-glycoprotein inhibition, Human Intestinal Absorption (HIA), skin permeability, plasma protein binding, Ames test for mutagenicity, lead-like rule, CMC-like rule. ADMET properties were investigated for the CYC molecule and listed in Table 5. The obtained BBB value for the CYC molecule is 0.3849, which shows that the molecule give rise to less side effects in the central nervous system [52]. In human skin, the permeability score value for CYC is -3.9795 cmh^{-1}. Human Intestinal Absorption (HIA) value for CYC is 94.322, predicted parameters were important and convenient to find out orally bioactive compounds and move the drug candidate to the next step [53]. The lead-like rule has higher binding affinity greater than 0.1μM. As per the CMC-like rule [54] in Table 5 and based on the ADMET properties, CYC molecule can be utilized in effective medications in future.

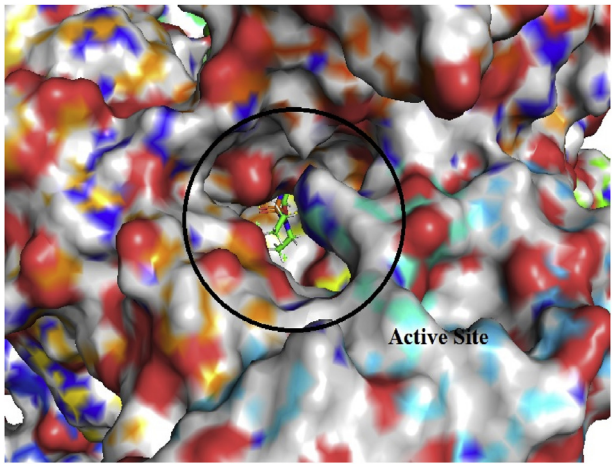

Figure 9. Surface view of CYC molecule embedded in the active site of the PI3K/AKT inhibitor.

4.10. Drug-likeness properties

To evaluate drug likeness of chemical compound, it should be formulated by using Lipinski's rule of five [55, 56]. The parameters obtained from the CYC are estimated by checking varieties in concentration of the medication that are easy to access. So overall sign of the conduct of the drug in the body; the parameters are given in Table 6. As indicated by Lipinski's rule of five, Hydrogen bond donor were found to be 1 ($\leq$5) and Hydrogen bond acceptor were found to be 4 ($\leq$10) respectively. The most important parameter is M logP that shows the similarity idea to the lipophilic character of the molecule which is shown as 2.66 under study, Topological polar surface area (TPSA) value for CYC is 41.57 $Å^2$ ($\leq$120 $Å^2$). The CYC molecule exhibits drug likeness properties as all the essential values estimated are in well preferred region. The bioactivity score for CYC molecule is measured and tabulated in Table 6, it can be seen that the CYC molecule concurs all the above expressed conditions and hence it is secure for use.

4.11. Molecular docking analysis

Molecular docking is very important role in the field of structural molecular biology, pharmacokinetics and structure based drug designing. The protein-ligand complex can be figured out effectively with molecular docking. The target protein PI3K/AKT was obtained from Protein data bank with PDB ID: 4JPS [57]. The resolution of protein with

Table 8. The amino acid residues in the binding cavity of PI3K/AKT protein which contributes more interaction other than hydrogen bonding interactions of CYC molecule.

CYC	PI3K/AKT amino acid residue and identifier	Distance
C1	Leu 814/2HB	3.0
C2	Met 811/HA	3.2
C3	Met 811/O	3.1
	Ile 633/2HD1	3.1
O12	Arg 818/1HH2	2.4
P13	Arg 818/1HH1	3.2
	Gly 837/2HA	2.9
N10	Gly 837/2HA	2.4
	Cys838/HN	2.6
O29	Cys 838/HN	2.3
N14	Arg 818/1HH1	3.4
C15	Arg 818/2HH2	3.0
C24	Leu 755/O	3.4
Cl28	Leu 755/O	3.4
Cl27	Leu 839/O	3.5
H11	Arg 818/1HH1	2.0
H6	Leu 814/2HB	2.0
H5	Cys 838/HN	2.0
H4	Met 811/CA	3.1
H9	Gln 815/HA	2.9
H7	Ile 633/2HD1	3.1
H8	Ile 633/2HD1	2.2

2.2 Å was chosen for accurate information from the protein structure. The water molecules and ions are removed from the protein. Hydrogen atoms are added to the polar residues of the protein before docking. We used the grid resolution 1 Å. The grid box size was chosen for energy estimation of flexible ligand docking in which the parameters of x, y and z coordinates are 46, 52, and 48 respectively. The three dimensional structure of the ligand CYC was drawn using Chemcraft tool and optimized using Gaussian 09 program with B3LYP functional using the employing 6–311++G (d,p) level of theory. The prepared protein and optimized structure of ligand is docked using Auto Dock tool. In molecular docking study, the ligand CYC is interacted in the binding cavity of PI3K/AKT inhibitor where the residues Lys 802, Asp810, Tyr 836, Val 851 and Ser854 act as active residues. The binding affinity of the CYC ligand with PI3K/AKT inhibitor is -5.70 kcal/mol is listed in the Table 7. The position of the ligand CYC in the binding cavity of PI3K/AKT inhibitor and the interaction plot of hydrophobic and hydrogen bonds are presented in Figures 7 and 8. Surface view of CYC molecule embedded in the binding cavity of the P3K/AKT inhibitor is seen as Figure 9. The compound CYC has higher negative free energy value and holds good activity for P3K/AKT inhibitor. It has two strong hydrogen bonds with the residues Tyr 836 and Cys 838 of PI3/AKT inhibitor with bond length of 2.23 and 2.26 Å respectively. The amino acid residues in the binding cavity of PI3K/AKT inhibitor which contributes more interaction other than hydrogen bonding interactions are presented in Table 8. So the CYC ligand found to possess anti-Non Small Cell Lung cancer agent.

5. Conclusion

In the present work, molecular structure, vibrational frequency (FTIR, FT-Raman) and quantum chemical calculations studies have been formed on CYC in order to identify its structural and spectroscopic features. The title compound was theoretically refined using B3LYP functional with 6–311++G (d,p) level of theory and the optimized geometry are tabulated in comparison with the experimental XRD data and well examined. The calculated HOMO-LUMO energy gap reveals that the charge transfer is due to interaction within the molecule. Molecular Electrostic Potential (MEP) and Mulliken analysis of CYC represents that the negative potential site is nucleophilic attack, while the positive potential sites are around the electrophilic attack. The intermolecular interaction contacts 2D fingerprint plots of CYC molecule are analyzed by maximum contribution of H···H with 46.7% in the Hirshfeld surface area. Natural bond orbital revealed that the (P13–N14) σ to (P13–O29) π* interaction set out the strongest stabilization energy of the system. Based on the results obtained from ADMET and Lipinski's rule of five, the drug likeness properties, CYC molecule is found to be better candidate. Docking studies affirms that the CYC is a good biological anti-Non Small Cell Lung cancer agent with low binding energy value of -5.70 kcal/mol.

Declarations

Author contribution statement

M.Govindammal, M. Prasath: Conceived and designed the experiments; Performed the experiments; Analyzed and interpreted the data; Contributed reagents, materials, analysis tools or data; Wrote the paper.

Funding statement

This research did not receive any specific grant from funding agencies in the public, commercial, or not-for-profit sectors.

Competing interest statement

The authors declare no conflict of interest.

Additional information

Supplementary content related to this article has been published online at https://doi.org/10.1016/j.heliyon.2020.e04641.

References

[1] A. Jemal, F. Bray, M.M. Center, J. Ferlay, E. Ward, D. Forman, Global cancer statistics, CA Cancer J 61 (2011) 69–90.
[2] M. Haubitz, F. Bohnenstengel, R. Brunkhorst, M. Schwab, U. Hofmann, D. Busse, Cyclophosphamide pharmacokinetics and dose requirements in patients with renal Insufficiency, Kidney Int. 61 (2006) 1495–1501.
[3] S. Muthu, N.R. Sheela, S. Sampathkrishnan, Density functional theory and ab initio studies of vibrational spectra of 2-bis (2-chloroethyl) aminoperhydro-1,3,2- oxaza phosphorinane-2-oxide, Mol. Simulat. 37 (2011) 1276–1288.
[4] M. Steven, Grunberg. Cyclophosphamide and etoposide for non-small cell and small cell lung cancer, Drugs 3 (1999) 11–15.
[5] C. Pagnoux, Updates in ANCA-associated vacuities, European Journal Rheumatology 3 (2006) 122–133.
[6] N. Khan, F. Afaq, F.H. khusro, V. mustafs Adhami, Y. suh, H. mukhtar, Dual inhibition of posphaatidylinositol 3-kinase/AKT and mammalian target of rapamycin signaling in human non-small cell lung cancer by dietary Flavonoid Myricetin, Int. J Cancer. 130 (2012) 1695–1705.
[7] J. Yang, J. Nie, X. Ma, Y. Wei, Y. Peng, X. Wei, Targeting pi3k in cancer: mechanisms and advances in clinical trials, Mol. Canc. 18 (2019) 26.
[8] F.D. Fruman, C. Rommel, PI3K and cancer: lessons, challenges and opportunities, Nat.Rev.Drug discovery 13 (2014) 140–156.
[9] I.A. Mayer, C.L. Arteaga, The PI3K/AKT pathway a Target for cancer treatment, Annu. Rev. Med. 67 (2016) 11–28.
[10] C.J. OlgaSchuurbiers, H.A.M. JohannesKaanders, F.M. Henricusvan der Heijden, P.N. RichardDekhuijzen, J.G. WimOyen, The PI3-K/AKT-pathway and radiation resistance mechanisms in non-small cell lung cancer, J. Thorac. Oncol. 4 (6) (2009) 761–767.
[11] T. Tian, J. Sun, J. Wang, Y. Liu, H. Liu, Isoliquiritigenin inhibits cell proliferaction and migration through the PI3K/AKT signaling pathway in A54 lung cancer cell, Oncol Lett 16 (2018) 6133–6139.
[12] S. Wang, Y. Yan, Z. Cheng, Y. Hu, T. Liu, Sotetsuflavone suppresses invasion and metastasis in non-small-cell lung cancer A549 cells by reversing EMT via the TNα/NF-κB and PI3K/AKT signaling pathway, Cell DeathDiscov 4 (2018) (2018) 2–6.
[13] M. Govindammal, M. Prasath, S. Kamaraj, B. Sathya, Invivo, molecular docking, spectroscopy studies of (S)-2,3-Dihydro-5,7-dihydroxy-2(3-hydroxy-4-methoxy phenyl)-4H-1-benzopyran-4-one: a potential uptake PI3/AKT inhibitor, Biocatalysis and Agricultural Biotechnology 18 (2019) 101086.
[14] Julian Tirado-Rives, William L. Jorgensen, Performance of B3LYP density functional methods for a large set of organic molecules, J. Chem.Theory.Comput. 4 (2008) 297–306.

[15] M.J. Frisch, G.M. Trucks, H.B. Schlegel, G.E. Scuseria, J.V. Ortiz, J. Cioslowski, D.J. Fox, Gaussian 09, Revision E.01, Gaussian, Inc., Wallingford CT, 2009.
[16] M. Raja, R. Raj Muhamed, S. Muthu, M. Suresh, Synthesis, spectroscopy (FT- IR, FT-Raman, NMR, UV-Visible), first order hyperpolarizability, NBO and molecular docking study of (E)-1-(4-bromobenzylidene) semicarbazide, J. Mol. Struct. 1128 (2017) 481–492.
[17] M.H. Jamroz, Vibrational Energy Distribution Analysis. VEDA 4 program, Warasaw, Poland, 2004.
[18] Christina Susan Abraham, S. Muthu, Johanan Christian Prasana, B. Fathima Rizwana, Stevan Armakovic, J. Sanja, C. Armakovi, Vibrational and electronic absorption spectroscopic profiling, natural hybrid orbital, charge transfer, electron localization function and molecular docking analysis on 3-amino-3-(2-nitrophenyl) propionic acid, J. Mol. Struct. 1171 (2018) 733–746.
[19] Christina Susan Abraham a, Johanan Christian Prasana a, S. Muthu b, B. Fathima Rizwana, M. Raja, Quantum computational studies, spectroscopic (FT-IR, FT-Raman and UVeVis) profiling, natural hybrid orbital and molecular docking analysis on 2,4 Dibromoaniline, J. Mol. Struct. 1160 (2018) 393–405.
[20] Dennington Roy, Todd Keith, John Millam, GaussView, Semichem Inc., Shawnee Mission, KS, 2009.
[21] A.E. Reed, L.A. Curtiss, F. Weinhold, Intermolecular interactions from a natural bon orbital, donor e acceptor viewpoint, Chem. Rev. 88 (1988) 899–926.
[22] M.J. Turner, J.J. McKinnon, S.K. Wolff, D.J. Grimwood, P.R. Spackman, D. Jayatilaka, M.A. Spackman, CrystalExplorer17.5, University of Western Australia, 2017.
[23] G.M. Morris, R. Huey, W. Lindstrom, M.F. Sanner, R.K. Belew, D.S.I. Goodsel, A.J. Olson, Automated docking using a Lamarckian genetic algorithm and empirical binding free energy function, J. Comput. Chem. 19 (1998) 1639–1662.
[24] W.L. Delano, PyMol Molecular Graphics System, Delano Scientific, San Carlos, CA,USA, 2002.
[25] Xin Liu, et al., The structural basis of protein acetylation by the p300/CBP ranscriptional co activator, Nat. Lett. 451 (2008) 846–850.
[26] G. Peter Jones, Holger Thonnessn, Axel Fischer, Ion Neda, Reinhard Schmutzler, Jurgen Engel, Bernhard Kutscher, Ulf Niemeyer, The anhydroys racemate of the carcinostatic agent Cyclophosphamide and the bicyclic degradation product 1- (2-chloropholo[2,1-b] [1,3,2] oxazaphosphorine9-oxide, Acta.Cryst. 52 (1996), 2359-236.
[27] M. Muthukkumar, T. Bhuvaneswari, G. Venkatesh, C. Kamal, P. Vennila, Stevan Armakovic, SanjaJ. Armakovic, Y. Sheena Mary, C. YohannanPanicker, Synthesis, Characterization and computational studies of semicarbazide derivative, Jol.of.mole.structure. 272 (2018) 81–495.
[28] M. Prasath, M. Govindammal, B. Sathya, Spectroscopic investigations (FT-IR & FT-Raman) and molecular docking analysis of 6-[1-methyl-4-nitro-1H-imidazol-5yl) sulfonyl]-7H-purine, J. Mol. Struct. 1146 (2017) 292–300.
[29] Shargina Beegum, Y. Sheena Mary, C. YohannanPanicker, Stevan Armakovic, Sanja J. Armakovic, Mustafa Arisoy, Ozlem Temiz-Arpaci, Spectroscopic, antimicrobial and computational study of novel benzoxazole derivative, J. Mol. Struct. 1176 (2019) 881–894.
[30] Y. Sheena Mary, Pankaj B. Miniyar, Y. Shyma Mary, K.S. Resmi, C. Yohannan Panicker, Stevan Armakovic, Sanja J. Armakovic, Renjith Thomas, B. Suresh kumar, Synthesis and spectroscopic study of three new oxadiazole derivatives with detailed computational evaluation of their reactivity and pharmaceutical potential, J. Mol. Struct. 1173 (2018) 469–480.
[31] B.R. Raajaram, N.R. Sheela, S. Muthu, Investigation on 1-Acetyl-4(4-Hydro Xyphenyl pipperazine an anti-fungal drug by spectroscopic, quantum chemical Computations and molecular docking studies, J. Mol. Struct. 1173 (2018) 583–595.
[32] H. Tanak, F. Ersahin, E. Agar, O. Buyukgungor, M. Yavuz, Crystal structure of N- 2-Methoxyphenyl-2-oxo-5-nitro-1-benzylidenemethylamine, Anal. Sci. 24 (2008) 237.
[33] S. Sevvanthi, S. Muthu, M. Raj, Molecular docking, Vibrational spectroscopic studies of (RS)-2 (tertbutylamino)-1-(3-chlorophenyl) propan-1-one: a potential adrenaline uptake inhibitor, J. Mol. Struct. 1173 (2018) 251–260.
[34] S. Sakthivel, T. Alagesan, S. Muthu, C.S. Abraham, E. Geetha, Quantum mechanical ,spectroscopic study (FT-IR and FT-Raman), NBO analysis, HOMO-LUMO ,first order hyperpolarizability and docking studies of a non-steroidal anti-inflammatory compound, J. Mol. Struct. 1156 (2018) 645–666.
[35] N.B. Colthup, L.H. Daly, S.E. Wiberly, Introduction to Infrared and Raman Spectroscopy, third ed., Academic press, Boston, 1990.
[36] D.F.V. Lewis, C. loannides, D.V. Parke, Interaction of a series of nitriles with the alcohol-inducible isoform of P450: computer analysis of structured activity relationships, Xenobiotica 24 (1994) 401–408.
[37] G. Gece, The use of quantum chemical methods in corrosion sciences, Corrosion Sci. 50 (2008), 2981-2922.
[38] A. Jacob George, Johanan Christian Prasana, S. Muthu, Tintu K. Kuruvilla, S. Sevanthi, Rinnu Sara Saji, Spectroscopic (FT-IR, FT Raman) and quantum mechanical study on N-(2,6-dimethylphenyl)-2-{4-[2-hydroxy-3-(2-methoxy phenoxy) propyl]piperazin-1-yl}acetamide, J. Mol. Struct. 1171 (2018) 268–278.
[39] R. Hoffmann, Solids and Surfaces: A Chemist's View of Bonding in Extended Structures, VCH Publishers, New York, 1988.
[40] T. Hughbanks, R. Hoffmann, Chains of trans-edge-sharing molybdenum octahedra: metal-metal bonding in extended systems, J. Am. Chem. Soc. 105 (1983) 3528–3537.
[41] J.G. Małecki, Synthesis, crystal, molecular and electronic structures of thiocyanate ruthenium complexes with pyridine and its derivatives as ligands, Polyhedron 29 (2010) 1973–1979.
[42] C. Morell, A. Grand, A.T. Labbe, Theoretical support for using the Df(r) descriptor, J. Chem. Phys. Let. 425 (2006) 342–346.
[43] P.W. Ayers, R. Parr, G. Parr, Variational principals for describing chemicalreactions: the Fukui function and chemical hardness revisted, J. Am. Chem. Soc. 122 (2000) 2010–2018.
[44] P. Chattaraj, K. Maiti, B. Sarkar, A unified treatment of chemical reactivity and selectivity, J. Phys. Chem. 107 (2003) 4973–4975.
[45] R. Meenashi, K. Selvaraju, A. David Stephen, Christian Jelsch, Theoretical crystal structure prediction of aminosalicylic acid: charge density topological and electrostatic analyses, J. Mol. Struct. 1213 (2020) 128139.
[46] Leila SeifikarGhomi, Mahdi Behzad, AtekehTarahhomi, Arab Ali, Crystal structures, DFT calculations, and Hirshfeld surface analyses of two new copper(II) and nickel(II) Schiff base complexes derived from meso-1,2-diphenyl-1,2-ethyl enediamine, J. Mol. Struct. 1150 (2017) 214–226.
[47] M.A. Spackman, J.J. McKinnon, Fingerprinting Intermolecular interactions in Molecular crystals, CrystEngComm 4 (2002) 378–392.
[48] P. Rajesh, P. Kandan, S. Sathish, A. Manikandan, S. Gunasekaran, S. Bala Abirami, Vibrational spectroscopic, UV-Vis, molecular structure and NBO analysis of Rabeprazole, J. Mol. Struct. 1137 (2017) 277–291.
[49] J. Liu, Z. Chen, S. Yuan, Study on the prediction of visible absorption maxima of Azobenzene compounds, J. Zhejiang Univ. - Sci. B. 6 (2005) 584–589.
[50] J. Lin, D.C. Sahakian, S. De Morais, J.J. Xu, R.J. Polzer, S.M. Winter, The role of absorption, distribution, metabolism, excretion and toxicity in drug discovery, Curr. Top. Med. Chem. 3 (2003) 1125–1154.
[51] J.C. Dearden, In Silico prediction of aqueous solubility, Exp Op Drug Disc. 1 (2006) 31–52.
[52] A.C. Mafud, M.P.N. Silva, G.P.L. Nunes, M.A.R. de Oliveira, L.F. Batista, T.I. Rubio, A.C. Mengarda, E.M. Lago, R.P. Xavier, S.J.C. Gutierrez, P.L.S. Pinto, A. da Silva Filho, Y.P. Mascarenhas, J. de Moraes, Antiparasitic, structural, Pharmacokinetic and toxicological properties of riparin derivatives, Toxicol. Vitro 50 (2018) 1–10.
[53] S. Sakkiah, C. Meganathan, Y.S. Sohn, S. Namadevan, K.W. Lee, Identification of Important chemical features of 11beta-hydroxysteroid dehydrogenase type1inhibitors: application of ligand based virtual screening and density functional theory, Int. J. Mol. Sci. 13 (2012) 5138–5162.
[54] C.A. Lipinski, Lead-and drug-like compounds: the rule-of-five revolution, Drug Discov. Today Technol. 1 (2004) 337–341.
[55] M.P. Postigo, R.V.C. Guido, G. Oliva, M.S. Castilho, I.R. Pitta, J.F. C de Albuquerque, et al., Discovery of new inhibitors of Schistosoma mansoni PNP by pharmacophore-based virtual screening, J. Chem. Inf. Model. 50 (2010) 1693–1705.
[56] C.A. Lipinski, F. Lombardo, B.W. Dominy, P.J. Feeney, Experimental and computational approaches to estimate solubility and permeability in drug.discovery and development settings, Adv. Drug Deliv. Rev. 23 (1997) 3–25.
[57] P. Furet, V. Guagnano, R.A. Fairhurst, P. Imbach-Weese, I. Bruce, M. Knapp, C. Fritsch, F. Blasco, J. Blanz, R. Aichholz, J. Hamon, D. Fabbro, G. Caravatti, Discovery of NVP-BYL719 a potent and selective phosphatidylinositol-3 kinase alpha inhibitor selected for clinical evaluation, Bioorg. Med. Chem. Lett 23 (2013) 3741–3748.